



HAL
open science

Phage-mediated intercellular CRISPRi for biocomputation in bacterial consortia

Abhinav Pujar, Amit Pathania, Corbin Hopper, Amir Pandi, Matthias Fugger, Thomas Nowak, Manish Kushwaha

► **To cite this version:**

Abhinav Pujar, Amit Pathania, Corbin Hopper, Amir Pandi, Matthias Fugger, et al.. Phage-mediated intercellular CRISPRi for biocomputation in bacterial consortia. 2024. hal-04699429

HAL Id: hal-04699429

<https://hal.science/hal-04699429v1>

Preprint submitted on 16 Sep 2024

HAL is a multi-disciplinary open access archive for the deposit and dissemination of scientific research documents, whether they are published or not. The documents may come from teaching and research institutions in France or abroad, or from public or private research centers.

L'archive ouverte pluridisciplinaire **HAL**, est destinée au dépôt et à la diffusion de documents scientifiques de niveau recherche, publiés ou non, émanant des établissements d'enseignement et de recherche français ou étrangers, des laboratoires publics ou privés.



Distributed under a Creative Commons Attribution - NonCommercial 4.0 International License

1 **Title**

2 Phage-mediated intercellular CRISPRi for biocomputation in bacterial consortia

3

4 **Authors**

5 Abhinav Pujar¹, Amit Pathania¹, Corbin Hopper^{1,2,3}, Amir Pandi¹, Matthias Függer^{2*}, Thomas
6 Nowak^{2,4*}, Manish Kushwaha^{1*}

7

8 ¹ Université Paris-Saclay, INRAe, AgroParisTech, Micalis Institute, 78352 Jouy-en-Josas,
9 France.

10 ² Université Paris-Saclay, CNRS, ENS Paris-Saclay, Laboratoire Méthodes Formelles, 91190
11 Gif-sur-Yvette, France.

12 ³ Université Paris-Saclay, CNRS, Laboratoire Interdisciplinaire des Sciences du Numérique,
13 91405 Orsay, France.

14 ⁴ Institut Universitaire de France.

15

16 *To whom correspondence should be addressed: mfuegger@lmf.cnrs.fr,
17 thomas@thomasnowak.net, or manish.kushwaha@inrae.fr

18

19 **Abstract**

20 Coordinated actions of cells in microbial communities and multicellular organisms enable
21 them to perform complex tasks otherwise difficult for single cells. This has inspired biological
22 engineers to build cellular consortia for larger circuits with improved functionalities, while
23 implementing communication systems for coordination among cells. Here, we investigate the
24 signalling dynamics of a phage-mediated synthetic DNA messaging system, and couple it with
25 CRISPR interference to build distributed circuits that perform logic gate operations in
26 multicellular bacterial consortia. We find that growth phases of both sender and receiver cells,
27 as well as resource competition between them, shape communication outcomes. Leveraging
28 the easy programmability of DNA messages, we build 8 orthogonal signals and demonstrate
29 that intercellular CRISPRi (i-CRISPRi) regulates gene expression across cells. Finally, we
30 multiplex the i-CRISPRi system to implement several multicellular logic gates that involve up
31 to 7 cells and take up to 3 inputs simultaneously, with single- and dual-rail encoding: NOT,
32 YES, AND, and AND-AND-NOT. The communication system developed here lays the
33 groundwork for implementing complex biological circuits in engineered bacterial communities,
34 using phage signals for communication.

35 Introduction

36 Over the past two decades, synthetic biology has advanced the ability of engineered
37 biological systems to sense environmental information and respond in a programmed manner.
38 These capabilities have found applications in detecting pollutants¹ and disease biomarkers²,
39 smart therapeutics³, and information processing logic circuits^{4–6}. This has been made possible
40 by designing genetic circuits using molecular components such as biosensors, transcription
41 factors, regulatory RNAs, riboswitches, or CRISPR systems for “internal wiring”^{7,8}. While most
42 engineered circuits are unicellular, the number of multicellular designs has been gradually
43 increasing due to their several advantages^{9–11}, including reduced metabolic burden due to
44 division of labour, minimised cross-talk, specialised sub-functions, distributed information
45 processing, concurrency, redundancy, and fault tolerance¹². These properties contribute to the
46 notion of “cellular supremacy” in biocomputing¹³, whereby multicellular circuits are expected
47 to enable more complex information processing¹⁴.

48 However, multicellular circuits do introduce additional challenges, such as the need to
49 balance populations of co-cultured cells that communicate through “external wiring”. To
50 establish communication channels between cells in these circuits, several natural signalling
51 molecules have been exploited; for example, homoserine lactones (HSL) from bacterial
52 quorum sensing systems¹⁵, yeast pheromones from mating signalling¹⁰, and mammalian
53 surface receptor-ligand pairs¹¹. Additionally, non-signalling molecules like secondary
54 metabolites and synthetic coiled-coil peptides have been repurposed for signalling^{16,17}. Despite
55 these developments, the current repertoire of communication molecules—four HSLs¹⁵, three
56 pheromones^{10,18}, two receptor-ligand pairs¹¹, six metabolites¹⁶, and two coiled-coil ligands¹⁷—
57 remains limited in both orthogonality and information capacity for higher-order multicellular
58 circuits.

59 In nature, intercellular communication is not confined to small molecules but extends to
60 information-rich nucleic acid molecules (DNA or RNA) transferred through cell junctions and
61 vesicles¹⁹, or mechanisms of horizontal gene transfer²⁰: transformation, conjugation, and
62 transduction. These nucleic acid messages can confer new functions on receiver cells^{21,22},
63 and can be rationally engineered to generate new orthogonal variants with altered
64 specificities^{23,24}. For instance, DNA delivery via conjugation has been used to modify
65 undomesticated bacteria²⁵, target pathogenic strains²⁶, and selectively deliver DNA messages
66 to specific cells within a population²⁷. Similarly, DNA delivery via bacteriophages has been
67 utilised for phage therapy²⁸, inactivation of antimicrobial resistance²⁹, microbiome editing^{30,31},
68 and metabolic pathway introduction³². Despite their potential, phages are not commonly used
69 for DNA propagation, possibly because most lyse their host cells upon release³³. Some
70 exceptions are the non-lytic filamentous phages, which continuously secrete from infected
71 cells, transmitting packaged DNA to new susceptible hosts³⁴. Of these, the M13 phage has
72 been extensively studied³⁵, and is widely used for applications in nanotechnology³⁶, phage
73 display³⁷, vaccine development³⁸, biosensing³⁹, and directed evolution^{40,41}.

74 In fact, M13 was also used in the first demonstration of DNA-based communication for a
75 multicellular circuit⁴². This pioneering work from over a decade ago delineated a key property
76 of nucleic acid signalling, “message-channel decoupling”⁴², by which multiple message
77 variants can be transmitted through a single communication channel. Despite this early
78 advance, progress in M13-mediated DNA messaging has been limited. Possible challenges

79 include its low adsorption rates⁴³, secretion heterogeneity⁴⁴, metabolic burden of infection⁴⁵,
80 and superinfection immunity that prevents multiple phages from infecting the same cell⁴⁶.

81 In this study, we engineered two M13 phagemid variants (*-gp3 ϕ* and *+gp3 ϕ*), suited for
82 different applications, and investigated how cell growth phase determines phage secretion
83 and infection kinetics. We studied how phage particle concentration and receiver cell density
84 impact infection rates in a well-mixed culture. These insights were used to implement a cell-
85 to-cell communication system, quantifying its communication kinetics in a co-culture with
86 resource competition. Next, we applied the phage communication system to engineer
87 intercellular CRISPR interference (i-CRISPRi), where a single guide RNA (sgRNA) gene
88 encoded on a phagemid is transmitted from a sender cell to a receiver cell, regulating gene
89 expression across the extracellular space. We quantified the CRISPRi gene regulation kinetics
90 for both isolated phages and sender cells. Finally, we demonstrated the multiplexing capability
91 of the i-CRISPRi system by building multicellular logic gates with up to seven cells, and
92 accepting single (NOT, YES), double (AND), and triple (AND-AND-NOT) senders as input.

93

94

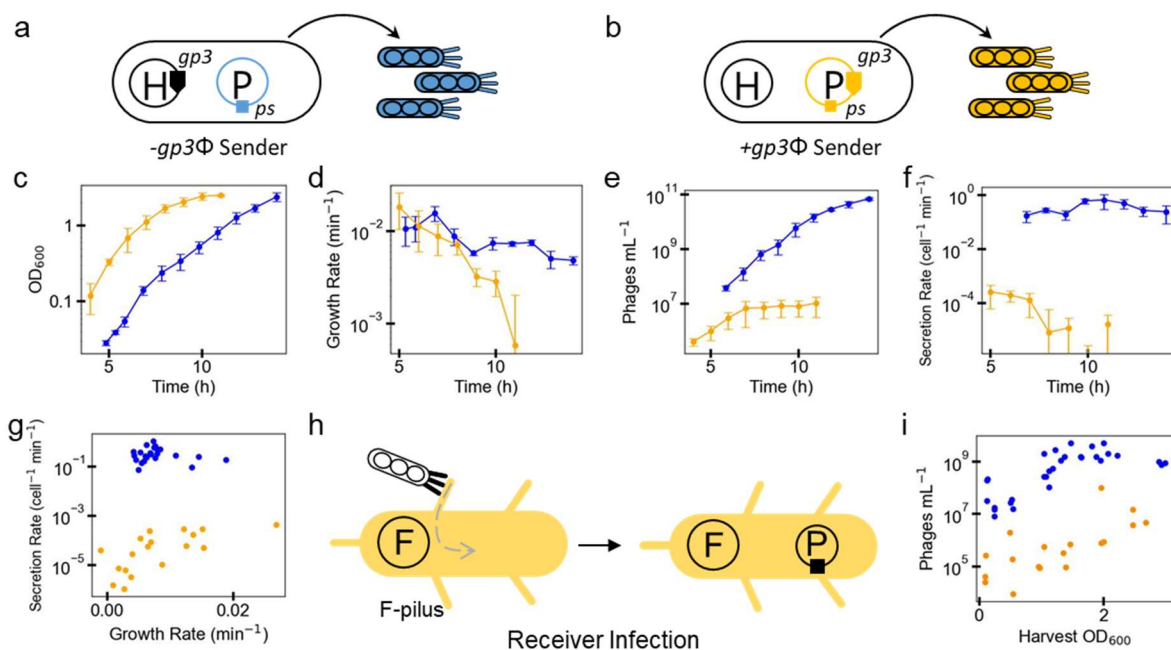
95

96 Results

97 Sender physiology impacts phage secretion rates

98 Many previous studies have examined the infection and secretion kinetics of the wild-type
99 M13 phage³⁵. In this study, however, we investigate the secretion kinetics of M13 phages
100 produced by engineered sender cells. Similar to prior works⁴², our senders contain two
101 plasmids: a helper (H) encoding the functional M13 proteins (gp1-gp11) and a phagemid (P)
102 carrying the M13 packaging signal (*ps*) for packaging and secretion. For some applications, a
103 phage without re-secretion suffices²⁸, while others require amplification through re-secretion⁴⁰.
104 We constructed two sender variants to compare: -gp3 Φ for delivery only, and +gp3 Φ for
105 delivery and re-secretion. Both variants have a *kanR* gene on the phagemid and constitutively
106 secrete phage particles. They differ in whether the minor coat protein *gp3* gene is encoded
107 on the helper or on the phagemid (**Fig. 1a and 1b**).

108 To study the kinetics of secretion, we monitored sender cultures for ~15 hours, measuring
109 OD₆₀₀ and collecting phage samples at 1 h intervals (**Fig. 1c and 1e**). -gp3 Φ and +gp3 Φ phages
110 were quantified using an assay for colony-forming units (CFU) or plaque-forming units (PFU),
111 respectively (**Fig. 1e**). -gp3 Φ phages cannot repackage inside receiver cells due to the
112 absence of the essential *gp3* gene, while +gp3 Φ phages can re-secrete if receivers have the
113 complementary phage machinery. Consequently, -gp3 Φ phages are quantified using CFU
114 assay whereas +gp3 Φ phages can be quantified using both CFU and PFU assays (see **Note**
115 **S1** for differences between CFU and PFU assays).



116 **Fig. 1: Secretion and infection kinetics of M13 phages are growth-phase dependent.** (a-b) Schematics of
117 phage-secreting sender cell variants: (a) -gp3 Φ (TOP10_H_Kan Φ) and (b) +gp3 Φ (TOP10_H Δ gIII_gIII-Kan Φ)
118 sender. Both variants carry an M13 helper plasmid (H) that encodes the phage machinery and a phagemid (P),
119 carrying a packaging signal (*ps*) for secretion. The essential minor coat protein gene, *gp3*, is encoded on the helper
120 in the -gp3 Φ sender and on the phagemid in the +gp3 Φ sender. (c) Growth curves of -gp3 Φ senders (blue) and
121 +gp3 Φ senders (orange), plotted as OD₆₀₀ against time. (d) Instantaneous growth rates of the two senders plotted
122 against time, calculated between each pair of consecutive time-points from the growth data in (c). (e) Phage
123 secretion curves of -gp3 Φ and +gp3 Φ senders plotted as phage titres against time. Titres of phages obtained from
124

125 the sender time-points in (c) were estimated using a CFU assay (-gp3φ) or a PFU assay (+gp3φ). (f) Instantaneous
126 secretion rates were calculated for each consecutive time-point pair from secretion curves obtained in (e). Data in
127 (c)-(f) show mean±SD from N=3 repeats. (g) Instantaneous secretion rates from (f) plotted against instantaneous
128 growth rates from (d). (h) Schematic of a phage particle infecting a receiver cell. The receiver carries an F-plasmid
129 encoding the F-pilus, the primary receptor for M13 phage infection. (i) Receiver cells (ER2738F) harvested at
130 different growth phases (harvest OD₆₀₀) were re-adjusted to the same density, and infected with the same number
131 of isolated phage particles (-gp3φ or +gp3φ). The number of infected cells were counted using a CFU assay (filled
132 circles) or a PFU assay (empty circles). Data in (i) show individual points from N=3 repeats.

133 Although both sender variants reached similar end-point ODs, -gp3φ senders had a longer
134 lag phase compared to +gp3φ senders (Fig. 1c). -gp3φ senders showed a higher
135 instantaneous growth rate (Fig. 1d), and produced 4 orders of magnitude more phages at the
136 end-point than +gp3φ senders (Fig. 1e). The per cell secretion rate of -gp3φ phages remained
137 relatively constant, while that of +gp3φ phages decreased over time, with maximum secretion
138 rates of 0.66 and 0.0002 phages min⁻¹ cell⁻¹, respectively (Fig. 1f; see Note S2 for the
139 relationship between OD and sender cell numbers). Differences in secretion rates probably
140 stem from differences in expression levels of the *gp3* gene⁴⁷ from the different plasmids: helper
141 plasmid for -gp3φ (pBBR1, copy number 4.7⁴⁸) and phagemid for +gp3φ (pUC, copy number
142 8.9⁴⁸). These secretion rates are lower than the 2–6 phages min⁻¹ cell⁻¹ reported for wild-type
143 filamentous phages^{35,47}. Consistent with prior findings⁴⁹, we observe a positive correlation
144 between growth rates and secretion rates per cell (Fig. 1g), suggesting that higher growth
145 rates are required to support phage secretion. Both phages show a plateau in secretion rate
146 at a growth rate of 0.0073 min⁻¹ (0.44 h⁻¹), indicating that other bottlenecks limit secretion
147 beyond this growth rate. Overall, we find that secretion kinetics of M13 phages are specific to
148 each phagemid, and depend on sender cell growth phase and phage machinery expression
149 levels.

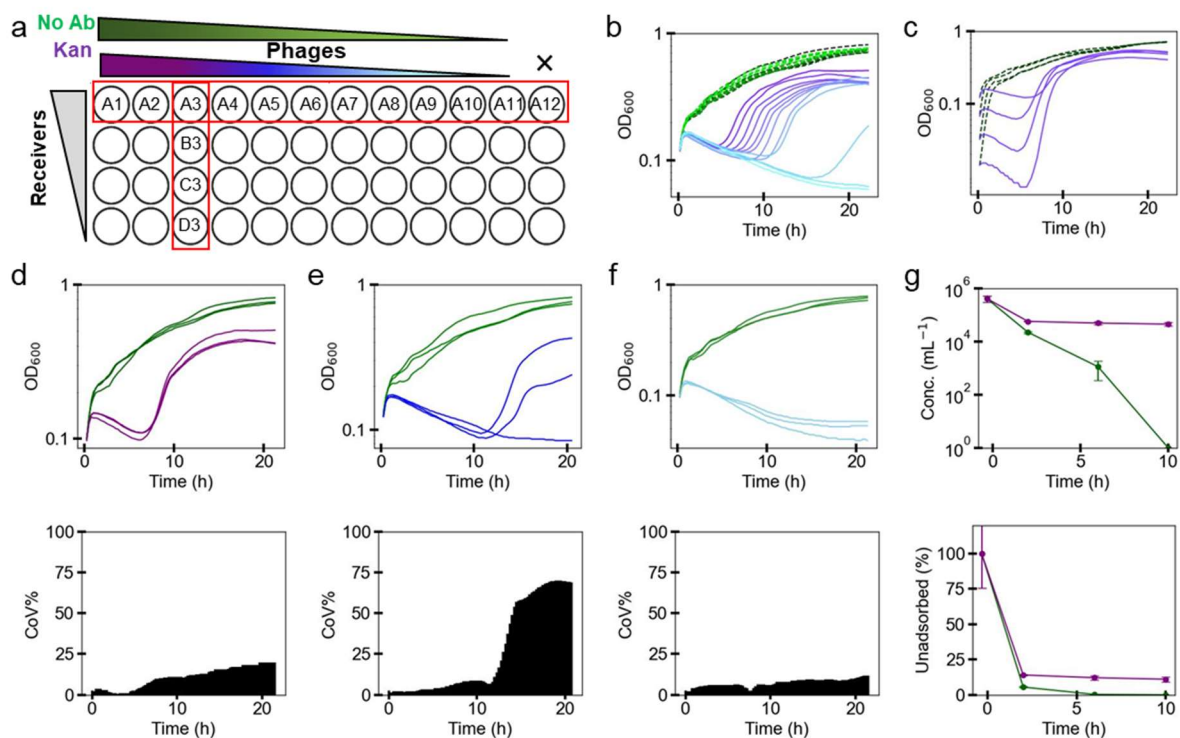
150 Receiver physiology impacts phage infection rates

151 Having established that the growth phase significantly affects sender cell secretion rates,
152 next we investigated its impact on receiver cell infection rates. Whereas in a growing batch
153 culture, cell density and growth phase vary simultaneously, we designed our experiments to
154 separate the two effects (Fig. 1i, S1.1-S1.2). Receiver cells were harvested at different ODs,
155 and resuspended to the same OD of 0.5, a commonly used density for PFU and CFU assays.
156 These resuspended cells were then infected with identical phage concentrations and counted
157 using a CFU assay for both -gp3φ and +gp3φ phages (Fig. 1h–i). Phage counts in the late
158 growth phase were 217-fold higher for -gp3φ and 323-fold higher for +gp3φ phages than in
159 the early growth phase, despite the same receiver cell OD. This suggests that receiver cells
160 at different phases of growth have different infectability, possibly due to more phage receptors
161 (F-pili) per cell in the late-log to early stationary phase⁵⁰. However, this effect is not apparent
162 when using PFU assays (Note S1).

163 To assess the effect of receiver density on infection, cells were grown to an OD ~1,
164 harvested, and resuspended to five different ODs before infection with the same phage
165 concentrations using a CFU assay (Fig. S1.2). Consistent with the law of mass action, higher
166 receiver densities resulted in more infected cells (CFU counts). Together, these findings
167 emphasise the impact of receiver cell physiology and density on infection rates, as well as the
168 limitations of the CFU method in accurately quantifying phage numbers (Note S1).

169 The role of stochastic interactions in infection dynamics of growing receiver cells

170 After examining the effects of physiology and density on receiver infection independently
 171 (Fig. 1), we investigated how phage infection impacts growing receiver cells in batch cultures
 172 where both factors change simultaneously. We used the +gp3 ϕ phage that can infect receiver
 173 cells only once (Fig. S3.1a), due to superinfection immunity from gp3 expression in
 174 receivers⁴⁶. Receiver cells at four starting densities (OD₆₀₀: 0.25, 0.125, 0.0625, 0.03125) were
 175 incubated with 12 concentrations of isolated phages (fold-dilutions: 3⁰ to 3¹⁰, and no-phage
 176 control) for 20 minutes in a 96-well plate (Fig. 2a), followed by growth with or without antibiotic
 177 selection (kanamycin) for ~20 hours (Fig. S4.1).



178 **Fig. 2: Phage infection dynamics in growing receiver cells.** (a) A schematic of the experimental setup. Different
 179 concentrations of isolated phages (+gp3 ϕ) were incubated with receiver cultures (ER2738F) at different densities
 180 in a 96-well plate for 20 mins without selection, and subsequently grown with (purple to sky blue) or without (green to light green)
 181 antibiotic (kanamycin) selection for infected receivers for ~20 hours (Fig. S4.1). (b) Growth curves
 182 of receiver cells incubated with varying concentrations of purified phages (wells A1–A12), plotted as OD₆₀₀ against
 183 time. (c) Growth curves of receiver cells at varying starting densities incubated with a fixed concentration of isolated
 184 phages (wells A3–D3), plotted as OD₆₀₀ against time. N=1 for (b) and (c). (d-f) (top panel) Repeats of growth curves
 185 from wells A4, A9 and A12 (includes data from (b)), plotted as OD₆₀₀ against time (bottom panel) Coefficients of
 186 variation (CoV) from the growth curve repeats in the top panel, plotted as CoV against time. Data in (d)-(f) are from
 187 N=3 repeats. (g) (top panel) Number of unadsorbed phages over time and (bottom panel) %unadsorbed phages
 188 over time in well D3, grown with (purple) or without (green) antibiotic selection. Data from N=3 repeats. (b-g) use
 189 the colour code defined in (a).
 190

191 With antibiotic selection, we observed a phage dose-dependent bacterial growth rescue at
 192 a fixed starting receiver density (Fig. 2b, S4.2). When the same number of phages were
 193 incubated with different densities of receiver cells, a similar growth rescue dependent on
 194 receiver density was observed (Fig. 2c, Fig. S4.3). Repeating these experiments three times
 195 with a subset of phage dilutions (3¹, 3², 3³, 3⁸, 3⁹, 3¹⁰) confirmed that growth rescue
 196 is more likely at higher phage concentrations (= lower dilutions) across all receiver densities

197 (**Fig. 2d-f**, top panel; **Fig. S4.4**). This is also indicated by the lower coefficients of variation
198 (%CoV) at higher phage concentrations (**Fig. 2d-e**, bottom panel; **Fig. S4.5**). These
199 differences in growth rescue reflect varying probabilities of infection across different phage-
200 receiver concentration settings.

201 We visualised growth rescue variability using heatmaps of %CoV at the 18 h end-point (**Fig.**
202 **S4.6**) and cumulative %CoVs over time (**Fig. S4.7**). Both heatmaps confirmed that infection
203 variability is lower at high phage concentrations and higher at low phage concentrations.
204 Interestingly, variability peaked at low phage and low receiver concentrations (**Fig. S4.6** and
205 **S4.7**), before reducing again at the lowest receiver OD of 0.03. This indicates that infection
206 probabilities are in the stochastic regime when phage and receiver concentrations are low. At
207 high phage and high receiver numbers, infection probability is high; at low phage and very low
208 receiver numbers, the infection probability is low, with both these conditions representing
209 deterministic infection regimes.

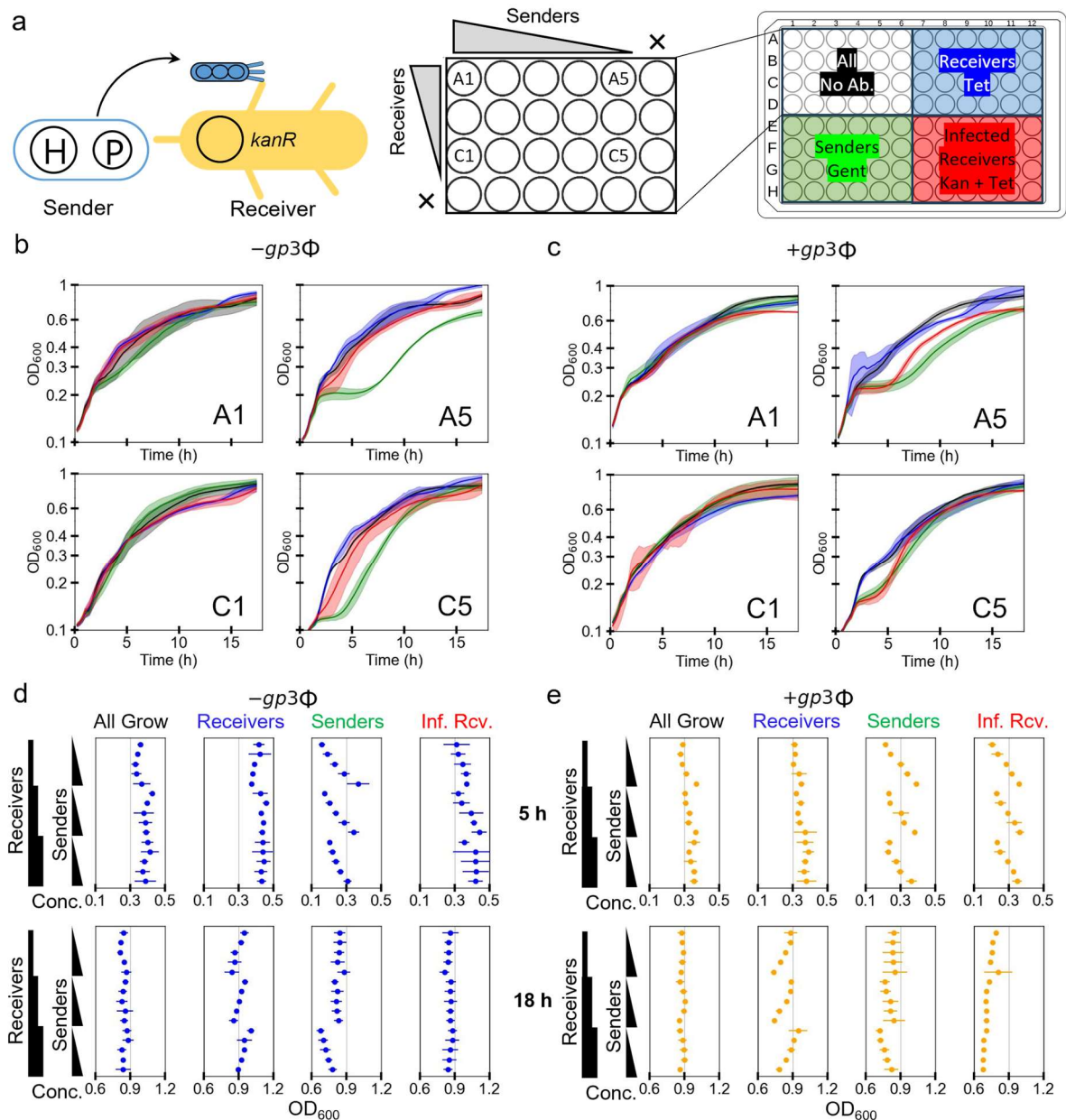
210 To observe phage uptake rates, we quantified unadsorbed phages from wells A3–D3 (**Fig.**
211 **2a**, phage dilution 3^2) at 2, 6, and 10 hours (**Fig. 2g**). In kan(-) wells, phages were
212 progressively adsorbed until almost none remained by 10 hours, driven by continuous
213 multiplication of uninfected receiver cells. In kan(+) wells, ~85% of phages were adsorbed
214 within 2 hours, with no further change later, indicating that uninfected cells were killed by
215 kanamycin, and only infected receivers grew thereafter (**Fig. 2g, S4.8**). The absence of further
216 phage depletion in kan(+) wells also suggests that phage depletion primarily occurs due to
217 adsorption by uninfected receiver cells, not repeat adsorption by infected receivers.

218 **Resource competition and antibiotic selection during communication between sender** 219 **and receiver cells**

220 Processes of horizontal gene transfer transmit valuable functions encoded on DNA
221 from one cell to another. When these cells compete for growth in the same environment,
222 competition for growth can affect the recipient's ability to take advantage of the newly acquired
223 functions⁵¹. Using a synthetic setup, we next studied intercellular communication dynamics
224 between phage-secreting sender and susceptible receiver cells in a co-culture. Senders (-
225 gp3φ and +gp3φ) and receivers were co-incubated without antibiotics for 1 h, followed by
226 growth under four conditions: without antibiotics, or with antibiotics to select for receivers only
227 (tetracycline), senders only (gentamycin), or infected-receivers only (kanamycin+tetracycline)
228 (**Fig. 3a, Note S5**).

229 Growth dynamics in these conditions revealed how resource competition and antibiotic
230 selection impacted communication (**Fig. 3b-c, S5.1, S5.4**). Without antibiotic selection, both
231 senders and receivers showed a monophasic growth. Similarly, growth in the receivers only
232 condition showed monophasic growth indicating that senders are rapidly killed by tetracycline,
233 and subsequent growth is by receivers only. In co-cultures where two cell types compete for
234 the same resources, biphasic growth curves often reflect sequential dominance due to the
235 initial growth of one cell type followed by the subsequent growth of the second one⁵², with a
236 biphasic lag between the two growth phases. Such biphasic growth is seen in the senders
237 only (gentamycin) condition, and is especially apparent when starting sender OD is low (**Fig.**
238 **S5.1**). As gentamycin killing of receiver cells is slow, they grow for some time while competing
239 with the senders for nutritional resources before dying. Therefore, wells with more starting
240 receivers (A5) show the biphasic lag later than those with fewer starting receivers (C5), even

241 when the starting senders in the two wells are the same. These observations are broadly
 242 similar between the $-gp3\phi$ and $+gp3\phi$ senders (Fig. S5.1 & S5.4). Biphasic growth was also
 243 observed in infected-receivers only (kanamycin+tetracycline) conditions, especially for $+gp3\phi$
 244 senders. This is because the secretion rates of $+gp3\phi$ senders are lower than those of $-gp3\phi$
 245 senders (Fig. 1f), resulting in more receivers remaining uninfected at the end of the 1 h pre-
 246 selection incubation. In the $-gp3\phi$ case, more receivers are infected before the selection is
 247 applied, allowing them to quickly outcompete both senders and uninfected receivers without
 248 an apparent biphasic lag.



249 **Fig. 3: Phage-mediated communication of DNA messages from growing senders to growing receivers. (a)**
 250 A schematic of the experimental setup. Sender ($-gp3\phi$ or $+gp3\phi$) and receiver cells were mixed at different starting
 251 densities in a 96-well plate, in four sets, and grown for 1 h without selection. Following that, different antibiotic
 252 selections were applied to three of the four sets to select for different cells: tetracycline for receivers only,
 253 gentamycin for senders only, and tetracycline+kanamycin for infected receivers only. For each set, initial sender
 254 (x-axis) and receiver densities (y-axis) were varied, starting from the undiluted ($OD_{600} = 0.136$), in 2-fold dilution
 255 steps, with the rightmost/bottommost column/row having no sender/receiver cells, respectively. **(b-c)** Growth
 256

257 curves of co-cultures in selected wells (A1, A5, C1, C5) plotted as OD₆₀₀ against time in all the four sets, with
258 different starting sender and receiver densities, using the colour code defined in (a). Data from *-gp3φ* senders are
259 in (b) and those from *+gp3φ* are in (c). (d-e) Plots of cell densities (OD₆₀₀) reached at a middle (5 h, top panel) and
260 the end (18 h, bottom panel) time-point in wells with different starting sender and receiver densities, under the
261 different selection conditions in the four sets. X-axis shows the density reached, and y-axis shows the starting
262 sender and receiver cell densities added. (d) and (e) show data from both *-gp3φ* and *+gp3φ* senders for growth in
263 the four selection conditions: no antibiotic (all cells), tetracycline (receivers only), gentamycin (senders only), and
264 tetracycline+kanamycin (infected receivers only). Data in (b)-(e) show mean±SD from N=3 repeats.

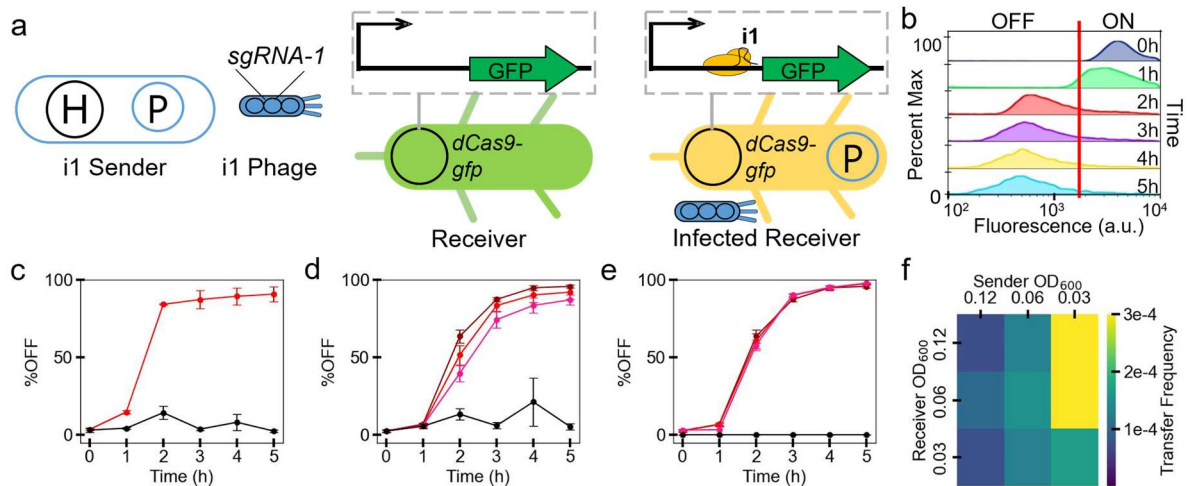
265 To further understand the contributions of sender and receiver numbers, we plotted
266 ODs of several wells at an early time-point (5 h) and the end-point (18 h) of post-selection
267 growth (Fig. 3d-e). More detailed plots are available in Note S5. Without antibiotics in the *-*
268 *gp3φ* experiments, wells with no receivers had lower end-point ODs than those with no
269 senders, suggesting that receivers, due to their higher growth rate, contributed more to the
270 final OD than senders (Fig. S5.2-S5.3). In the *+gp3φ* experiments, both senders and receivers
271 equally contributed to growth, resulting in similar end-point ODs (Fig. S5.5-S5.6) due to their
272 individual growth rates being more comparable (Fig. S5.9). In receiver only conditions, end-
273 point ODs in both *-gp3φ* and *+gp3φ* experiments were lower in wells with higher starting
274 senders (Fig. 3d-e). This is due to early resource competition between receivers and senders
275 before the latter are killed by tetracycline. In sender only conditions, ODs were higher at 5 h
276 in wells with more starting senders, but plateaued by 18 h with little dependence on starting
277 sender numbers (Fig. 3d-e). However, the effect of early resource competition with the
278 receivers was still visible, resulting in lower ODs in wells with higher starting receivers (Fig.
279 3d-e). Furthermore, the resource competition effect was much smaller in senders only data
280 than seen above in receivers only data, due to receivers being less rapidly killed by
281 gentamycin than senders are killed by tetracycline.

282 In the infected-receivers condition at an early time-point (5h), as expected the OD is
283 higher for wells with higher starting senders. This effect of sender dose dependence was more
284 pronounced for *+gp3φ* senders than *-gp3φ* senders (Fig. 3d-e), due to the former's lower
285 secretion rates that result in lower phage titres by the end of the 1 h incubation (Fig. 1f).
286 Variability between repeats in sender-receiver communication experiments (Fig. S5.7-S5.8),
287 for both senders, was lower than in phage-receiver infections (Fig. 2d-f, S4.5). We estimate
288 that <15 cells per mL of *-gp3φ* senders or <22000 cells per mL of *+gp3φ* senders would be
289 needed for sender-receiver infections to exhibit high variability similar to phage-receiver
290 infections. The end-point ODs plateaued if any senders were present, with higher ODs for *-*
291 *gp3φ* than *+gp3φ* senders. Within each set with fixed starting receivers, increasing sender
292 numbers reduced the end-point OD (Fig. 3d-e, S5.2, S5.5). For *-gp3φ*, the starting receiver
293 OD had little effect (Fig. S5.2), but for *+gp3φ*, higher starting receiver OD led to lower final OD
294 (Fig. S5.5). This is due to early resource competition with more receivers that later die if
295 uninfected. This suggests that when the phage-mediated communication rate is low (as for
296 *+gp3φ*), vertical transfer of the phagemid from mother to daughter cell is more efficient than
297 horizontal transfer from sender to receiver cell.

298 Intercellular gene regulation using CRISPRi circuits

299 Over the past decade, programmable CRISPR nucleases and their catalytically dead
300 mutants have been widely used in genome engineering and gene regulation applications⁵³.
301 CRISPR systems are standalone in their function, with the expression of the CRISPR nuclease

302 and guide RNA being sufficient for activity, even in heterologous settings or *in vitro*⁵³. The
 303 specificity of CRISPR systems can be programmed by modifying the guide RNA sequence to
 304 direct the ribonucleoprotein to a specific DNA or RNA target. This versatility has made
 305 CIRSPR systems valuable tools for building information processing genetic circuits^{8,23}, acting
 306 as internal wires in the cell, or function as DNA payload selectors²⁷.



307
 308 **Fig. 4: Phagemids encoding CRISPR single guide RNA can regulate receiver gene expression.** (a) A
 309 schematic of the intercellular CRISPR interference system. Sender i1 secretes phage particles encoding *sgRNA-1*.
 310 The phage particle infects a receiver cell (TOP10F_dCas9-GFP_NOT_i1), resulting in the delivery of the *sgRNA-1*
 311 encoding DNA that subsequently expresses *sgRNA-1* in the receiver cells. *sgRNA-1* forms a complex with available
 312 dCas9 and binds to the promoter region of *gfp*, causing repression. (b) Distribution of GFP fluorescence in receiver
 313 cells incubated with isolated *sgRNA-1* phages for varying durations of up to 5 h, without antibiotic selection. Number
 314 of GFP ON and OFF cells was determined using a fluorescence threshold value (vertical red line). These
 315 representative plots are from a single experiment (N=1). (c) Percentage of repressed (GFP OFF) cells in the
 316 receiver population, sampled every hour for 5 hours. Repression is shown from receiver cells with (red) or without
 317 (black) added phages. Data show mean±SD from N=3 repeats. (d-e) Receiver GFP repression across time is
 318 shown when incubated with *sgRNA-1* senders (TOP10_H_sgRNA-1_AmpΦ) without selection. Like in (c), the
 319 percentage of repressed receivers is plotted against time. Data in (d) are from a fixed starting receiver density
 320 (OD₆₀₀ = 0.125), and varying starting sender densities: OD₆₀₀ 0.125 (dark red), 0.0625 (red), 0.0312 (pink), no
 321 sender (black). Data in (e) are from a fixed starting sender density (OD₆₀₀ = 0.125), and varying starting receiver
 322 densities: OD₆₀₀ 0.125 (dark red), 0.0625 (red), 0.0312 (pink), no receiver (black). Data in (c)-(e) show mean±SD
 323 from N=3 repeats. (f) Heatmap showing transfer frequency (mL cell⁻¹) at 3 h of co-culturing, calculated for different
 324 starting sender and receiver ODs.

325 Building on the phage-mediated cell-to-cell communication (Fig. 3), we aimed to create
 326 multicellular circuits where DNA messages coding for CRISPR guide RNAs are secreted by
 327 sender cells and delivered by phages to modify receiver gene expression. We term this
 328 process "intercellular CRISPRi" (i-CRISPRi). We began by examining the infection dynamics
 329 and circuit response of a simple i-CRISPRi circuit (Fig. 4a) using the -gp3φ phagemid variant,
 330 which has a higher secretion rate and lacks superinfection inhibition. Co-transformation of the
 331 GFP-dCas9 plasmid, which constitutively expresses dCas9 and GFP, with a single guide RNA
 332 (*sgRNA*) expressing phagemid showed high repression of GFP (Fig. S6.1). Next, isolated
 333 *sgRNA-1* phages (3.6x10¹³ mL⁻¹, CFU assay) were incubated with receiver cells at 0.125 OD
 334 without antibiotic selection, GFP expression was monitored for 5 hours by flow cytometry, and
 335 receiver cells were gated into 'OFF' and 'ON' populations (Fig. 4b). DNA messages, unlike
 336 small molecules, behave like digital signals; a single successful transmission delivers the full
 337 message to the receiver cell where its expression can activate the downstream circuit. Infected

338 receivers expressing sgRNA-1 formed a dCas9-sgRNA complex that repressed the *gfp*
339 promoter, increasing the %OFF cells in the population (**Fig. 4c**). GFP expression was
340 repressed in 84% of receiver cells by 2 hours, and 90% cells by 5 hours. These results are
341 consistent with those reported in the first phage-derived DNA messaging system where 92%
342 receivers got infected by phages from sender cells within 5 h without antibiotic selection⁴².

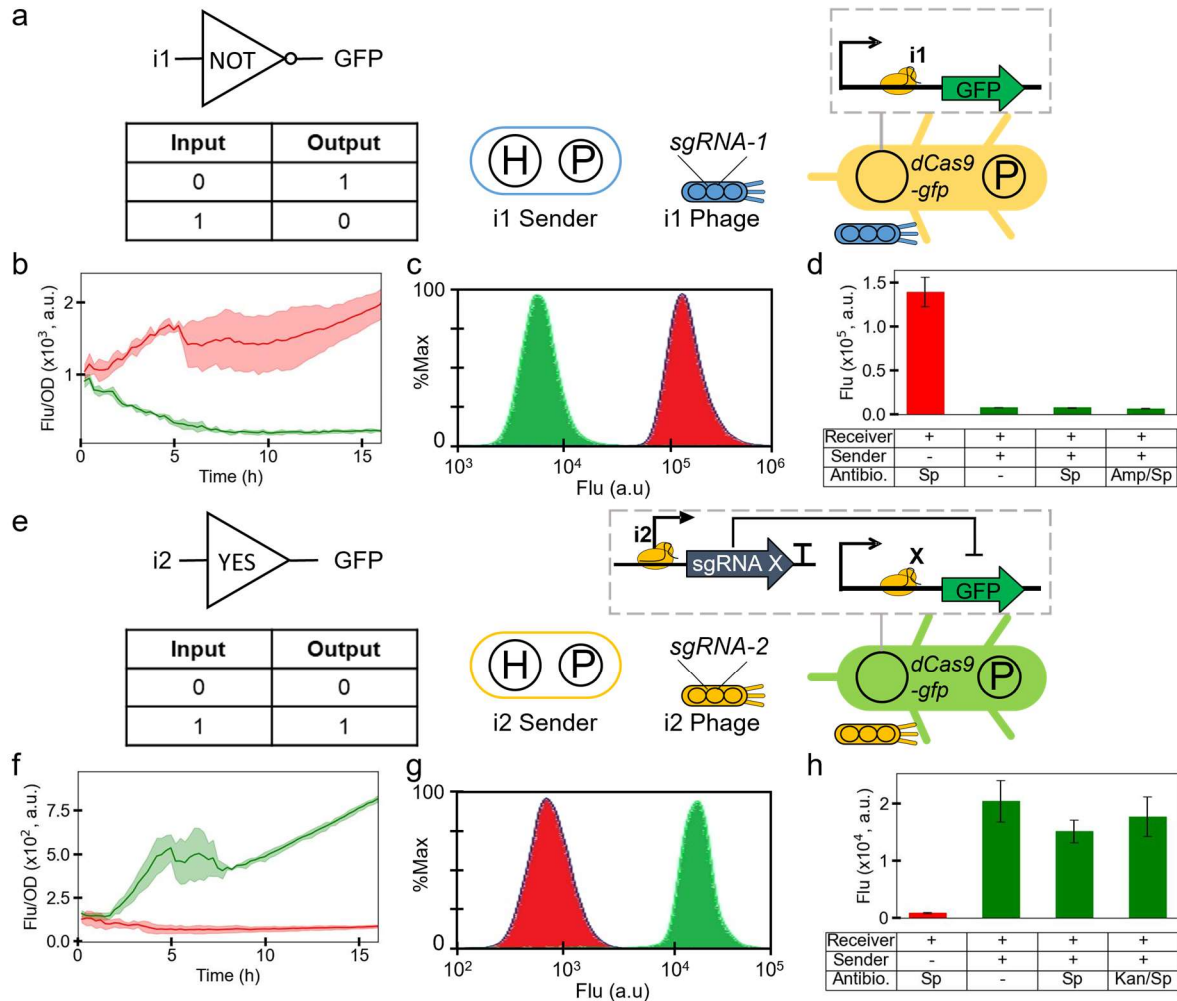
343 After confirming GFP repression by *sgRNA-1* in phage-transduced receiver cells, we
344 constructed the i-CRISPRi circuit with senders secreting the sgRNA phagemid and receivers
345 expressing dCas9 and GFP. Upon co-culturing of the sender and receiver cells, sgRNA
346 phages produced by the senders can transduce into the receivers (**Fig. S6.2**). Co-culturing
347 sender and receiver cells in varying ratios showed that 87% of receivers expressed ~20-fold
348 lower GFP at a 1:4 sender:receiver ratio within 5 hours (**Fig. 4d**). Higher sender ratios (2:4 or
349 4:4) further increased the GFP-repressed population to 92% and 95%, respectively.
350 Increasing sender numbers, while keeping the receiver numbers the same, slightly reduced
351 the time to repress 50% of receivers from 2.29 h (1:4 ratio) to 1.98 h (2:4 ratio) and 1.76 h (4:4
352 ratio). Sender:receiver ratios of 4:4, 4:2, and 4:1 showed no significant difference in repression
353 rates, suggesting excess phage secretion at those sender numbers (**Fig. 4e**).

354 We calculated the phagemid transfer frequency from senders to receivers, using a method
355 used to obtain transconjugation frequency in conjugation experiments²⁷. We found that the
356 highest transfer frequency of 3×10^{-4} mL cell⁻¹ was observed at 3 hours of co-incubation for low
357 sender and high receiver starting densities (**Fig. 4f, S6.3**). This transfer rate vastly exceeds
358 the 5.2×10^{-9} reported for transconjugation at 6 hours²⁷. Two additional i-CRISPRi circuit
359 variants with different sgRNA and cognate promoter sequences confirmed the general
360 applicability of these circuits (**Fig. S6.4, S6.5**). However, it also revealed differences in the
361 rate of GFP repression, possibly because the different replication origins used affect phage
362 communication rates.

363 **Single-input Boolean logic gates using intercellular CRISPRi**

364 After demonstrating i-CRISPRi regulation (**Fig. 4**), we designed multicellular circuits
365 implementing single-input Boolean logic gates. Previously, we had tested i-CRISPRi circuits
366 without antibiotic selection, but selection may be needed as circuit complexity and the number
367 of inputs increase. So, we examined how circuit output changes with and without selection for
368 two single-input gates: NOT and YES.

369 The NOT gate was built using sgRNA-1 encoding phagemid secreted by senders to
370 infect receiver cells expressing GFP and dCas9 (**Fig. 5a**). This circuit uses a "single-rail"
371 encoding, where the sender's presence represents input '1' and its absence represents input
372 '0'. Sender-receiver co-cultures were grown for 4 hours without selection, followed by 16 hours
373 of growth under four conditions: no antibiotic, selection for receivers only (spectinomycin),
374 senders only (gentamycin), and infected-receivers only (spectinomycin+ampicillin) (**Fig. 5b**,
375 S7.1). Flow cytometry showed that infected receivers exhibited a 21.3-fold decrease in GFP
376 expression compared to the uninfected receiver control (**Fig. 5c**). Interestingly, selection for
377 sgRNA phagemid was not necessary, as setups without antibiotics or selection for receivers
378 only (spectinomycin) showed similar results (**Fig. 5d, S7.2**).



379
 380 **Fig. 5: Intercellular CRISPRi for digit logic gates NOT and YES.** (a) Schematic of the intercellular CRISPR
 381 interference system for NOT logic gate behaviour. Sender i1 secretes phage particles encoding *sgRNA-1*. Upon
 382 infection and expression in the receiver cells, *sgRNA-1* represses *gfp* expression by CRISPRi. (b) NOT-gate
 383 uninfected receivers (red), and infected receivers (green), were grown for 16 hours in a plate reader, with OD₆₀₀
 384 and fluorescence recorded at regular intervals. A time-course of Fluorescence/OD is plotted here. (c) Distribution
 385 of GFP fluorescence in receiver cells incubated without or with *sgRNA-1* senders for 16 hours, with appropriate
 386 antibiotic selection (without sender = red, spec; with sender = green, spec+amp). These representative plots are
 387 from a single experiment (N=1). (d) Same experiment as in (c), except two additional growth conditions with
 388 senders are shown (no antibiotic and spec). Mean±SD of fluorescence data from N=3 repeats are plotted here. (e)
 389 Schematic of the intercellular CRISPR interference system for YES logic gate behaviour. Sender i2
 390 (TOP10_H_sgRNA-2_KanΦ) secretes phage particles encoding *sgRNA-2*. Upon infection and expression in the
 391 receiver cells (TOP10F_dCas9-GFP_YES_i2), *sgRNA-2* represses *sgRNA-X*, in turn depressing *gfp* expression.
 392 (f) YES-gate uninfected receivers (red), and infected receivers (green), were grown for 16 hours in a plate reader,
 393 with OD₆₀₀ and fluorescence recorded at regular intervals. A time-course of Fluorescence/OD is plotted here. (g)
 394 Distribution of GFP fluorescence in receiver cells incubated without or with *sgRNA-2* senders for 16 hours, with
 395 appropriate antibiotic selection (without sender = red, spec; with sender = green, spec+kan). These representative
 396 plots are from a single experiment (N=1). (h) Same experiment as in (g), except two additional growth
 397 conditions with senders are shown (no antibiotic and spec). Mean±SD of fluorescence data from N=3 repeats are plotted here.

398 The YES gate (buffer gate) circuit used sender cells encoding *sgRNA-2* and a receiver
 399 circuit with two sequential NOT gates (inverters) (Fig. 5e). Receiver cells carried the YES gate
 400 circuit on a plasmid expressing *sgRNA-X* and dCas9, with their complex repressing the GFP
 401 promoter. *sgRNA-X* promoter, in turn, was regulated by the *sgRNA-2*. YES gate sender and
 402 receiver cells were co-cultured for 4 hours without selection, followed by 16 hours under the

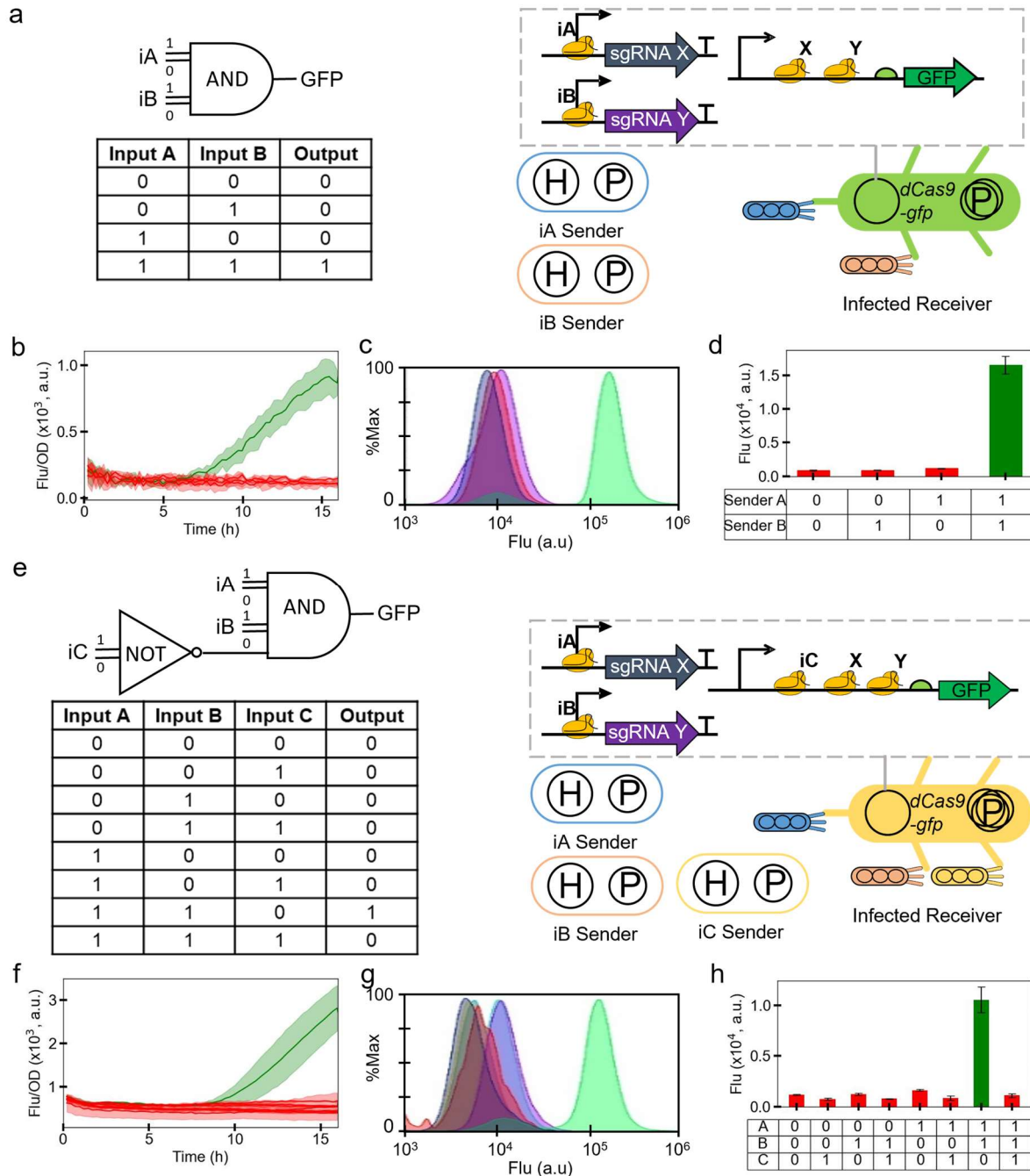
403 same four conditions used previously (**Fig. 5f**, S7.3). Flow cytometry showed a 20.7-fold
404 increase in GFP expression in infected receivers compared to the uninfected receiver control
405 (**Fig. 5g**). Similar to the NOT gate, selection for sgRNA was not required in the receiver cells
406 (**Fig. 5h**, S7.4). High GFP activation was observed after 16 hours without selection, but not
407 after 4 hours of pre-incubation (**Fig. S7.5**). This is different to the circuit behaviour previously
408 observed with the sgRNA-1 NOT gate senders (**Fig. 4d**), where 4 h of pre-incubation without
409 selection was already sufficient to reach 95% repression. This suggests either lower sgRNA-
410 2 phage secretion rates or a longer delay between infection and activation in the YES gate
411 circuit, or a combination of both.

412 Post-selection data showed that the YES gate fluorescence switch requires more time
413 than the NOT gate, where a response was seen almost immediately (**Fig. 5b**, 5f, S9.1).
414 Defining circuit switching time as a $\geq 20\%$ change from the no-input control fluorescence, the
415 NOT gate switch begins at 39.6 min, while the YES gate switch starts at 173.4 min (2.89 hours)
416 (**Fig. S9.1**). The longer YES gate switch time is likely due to the additional CRISPRi step in
417 the repression cascade.

418 **Multi-input Boolean logic gates using intercellular CRISPRi**

419 Before implementing multi-input logic gates, we checked if receiver cells could be infected
420 by multiple phages simultaneously. Receiver cells were incubated with 1, 2, or 3 phage types
421 (differing in replication origins and antibiotic markers) for 1 hour, then subjected to antibiotic
422 selection. Results showed that cells could be co-infected by multiple -gp3 ϕ phagemids
423 simultaneously (**Fig. S3.2**), but not if already infected with a +gp3 ϕ phagemid (**Fig. S3.1a**).
424 While multiple -gp3 ϕ infections are possible, multiple antibiotic selections reduced receiver
425 cell growth. Yet, given the lack of circuit activation at 4 h without selection seen earlier in the
426 YES gate (**Fig. S7.5**), antibiotic selection seems necessary if circuits are to be activated by
427 multiple inputs. However, comparing fluorescence output under different growth conditions is
428 challenging due to growth rate differences affecting GFP dilution⁵⁴. To address both these
429 requirements together, we used "dual-rail" encoding, where circuit input comes from two types
430 of sender cells delivering a '0' signal (dummy sgRNA) or a '1' signal (targeting sgRNA).

431 The AND gate (A.B) receiver uses a plasmid encoding GFP, dCas9, *sgRNA-X*, and *sgRNA-Y*.
432 In complex with dCas9, either of the two sgRNAs represses GFP by binding downstream
433 of the promoter (**Fig. 6a**). This promoter configuration with tandem repressor binding sites
434 behaves like a NOR gate, which owing to its functional completeness can be layered to build
435 any digital logic⁹. Promoters of *sgRNA-X* and *sgRNA-Y* are regulated by *sgRNA-A* and
436 *sgRNA-B*, respectively. Two sender cells secrete phages encoding *sgRNA-A* and *sgRNA-B*
437 for signal input '1' (TOP10_H_sgRNA-A1_Kan Φ and TOP10_H_sgRNA-B1_Gent Φ), while
438 two others secrete null phages encoding dummy sgRNAs for signal input '0'
439 (TOP10_H_sgRNA-A0_Kan Φ and TOP10_H_sgRNA-B0_Gent Φ). The '1' and '0' senders of
440 any input set are never used together. The AND gate was implemented in a 2-sender 1-
441 receiver circuit, incubated with all combinations of senders ('00', '01', '10', and '11') for 4 hours
442 without selection, then grown for 16 hours with multi-antibiotic selection in a plate reader (**Fig.**
443 **6b**, S8.1). Flow cytometry showed a 17-fold increase in fluorescence with the '11' sender
444 combination compared to the mean of the other three combinations (**Fig. 6cd**, S8.2).



445
446
447
448
449
450
451
452
453
454
455
456
457
458
459

Fig. 6: Intercellular CRISPRi for digit logic gates AND and AND-AND-NOT. (a) Schematic of the intercellular CRISPR interference system for AND logic gate behaviour. Senders iA and iB secrete phage particles encoding either null (state '0') phages, or *sgRNA-A* and *sgRNA-B* (state '1') phages. Only upon infection of receiver cells by both state '1' phages, *sgRNA-A* and *sgRNA-B* repress *sgRNA-X* and *sgRNA-Y*, respectively, in turn depressing *gfp* expression. (b) AND-gate receivers (red) infected by non-activating combinations of phages (00, 01, 10), and receivers (green) infected by activating combination (11) of phages, were grown for 16 hours in a plate reader, with OD₆₀₀ and fluorescence recorded at regular intervals. A time-course of Fluorescence/OD is plotted here. (c) Distribution of GFP fluorescence in receiver cells incubated with *sgRNA-A* and *sgRNA-B* senders for 16 hours, with appropriate antibiotic selection. These representative plots are from a single experiment (N=1). (d) Same experiment as in (c), except the mean±SD of fluorescence data from N=3 repeats are plotted here. (e) Schematic of the intercellular CRISPR interference system for AND-AND-NOT logic gate behaviour. Senders iA, iB, and iC secrete phage particles encoding either null (state '0') phages, or *sgRNA-A*, *sgRNA-B*, and *sgRNA-C* (state '1'). Only upon infection of receiver cells by state '1' phages A and B and state '0' phage C, *sgRNA-A* and *sgRNA-B* repress *sgRNA-X* and *sgRNA-Y*, respectively, in turn depressing *gfp* expression. If state '1' phage C infects

460 receivers, it directly represses *gfp*. **(f)** AND-AND-NOT gate receivers (red) infected by non-activating combinations
461 of phages (000, 001, 010, 011, 100, 101, 111), and receivers (green) infected by activating combination (110) of
462 phages, were grown for 16 hours in a plate reader, with OD₆₀₀ and fluorescence recorded at regular intervals. A
463 time-course of Fluorescence/OD is plotted here. **(g)** Distribution of GFP fluorescence in receiver cells incubated
464 with sgRNA-A, sgRNA-B, and sgRNA-C senders for 16 hours, with appropriate antibiotic selection. These
465 representative plots are from a single experiment (N=1). **(h)** Same experiment as in (g), except the mean±SD of
466 fluorescence data from N=3 repeats are plotted here.

467 The AND-AND-NOT (A.B.~C) gate receiver (TOP10F_dCas9-GFP_AAN) has a circuit
468 plasmid with an sgRNA binding site downstream of the *gfp* promoter for repression by an
469 additional sgRNA-C produced by sender C (TOP10_H_sgRNA-C1_Amp Φ) (**Fig. 6e**). This
470 circuit involves three sender cells for signal '1' (sgRNA-A, sgRNA-B, sgRNA-C) and three for
471 signal '0' (dummy sgRNAs). The AND-AND-NOT gate was implemented in a 3-sender 1-
472 receiver circuit, tested with combinations ('000', '001', '010', '011', '100', '101', '110', '111') for
473 4 hours without selection, followed by 16 hours with antibiotics (**Fig. 6f**, S8.3). Using flow
474 cytometry, a 9.8-fold increase in GFP expression was observed between the ON-state ('110')
475 and the mean of all OFF-states (**Fig. 6gh**, S8.4). Senders A1, B1, and null sender C0
476 (TOP10_H_sgRNA-C0_Amp Φ) were incubated with receivers to achieve the ON-state.

477 The 20% switching response time increased to 8.52 hours for AND gate and 10.71 hours
478 for AND-AND-NOT gate compared to single-input circuits (**Fig. 5**, 6b, 6f, S9.1), due to the time
479 lag from additional CRISPRi steps required in the repression cascade (**Fig. S9.1**).

480

481

482

483 Discussion

484 In this work, we have leveraged key advantages of a phage-derived DNA messaging
485 system, high programmability and message-channel decoupling⁴², to implement several
486 distributed logic gates in multi-strain bacterial consortia. We investigated the transmission
487 (secretion) and reception (infection) dynamics of the messaging system, revealing that both
488 steps are significantly influenced by the growth phase of sender and receiver cells, though in
489 contrasting ways. Secretion rates decrease as senders transition from early to late growth
490 phases (**Fig. 1f**), whereas infection rates of receivers increase during a similar transition (**Fig.**
491 **1i**). This emphasizes the need to assess phage production and infection kinetics not just in
492 the exponential phase, as is commonly done, but across different growth phases. It is
493 especially relevant since bacteria in many natural environments exist in different phases of
494 growth with potentially different cell surface properties that influence phage infection^{55,56}.
495 Additionally, the phage yield and secretion rate varied between -gp3 ϕ and +gp3 ϕ sender
496 variants, suggesting that phage machinery expression level is crucial for optimal phage
497 production (**Fig. 1e-f**).

498 Studying phage infection kinetics in growing receiver cells, we found high infection
499 variability with low phage and receiver concentrations (**Fig. 2d-f, S4.5**). This is consistent with
500 previous findings that implicated stochastic phage-bacterial interactions, due to spatial
501 heterogeneity in the gut, for the poor efficacy of phage therapy⁵⁷. Using sender cells rather
502 than isolated phages reduced this variability substantially, due to phage dose amplification
503 (**Fig. S4.5, S5.7-5.8**). This suggests that using sender cells instead of isolated phages for
504 phage-mediated DNA delivery can improve outcomes in phage therapy and microbiome
505 editing applications. However, phage communication kinetics between senders and receivers
506 are shaped by resource competition among cells. Increasing sender ratios does not guarantee
507 more infected receivers, as too many senders can deplete the resources needed for receiver
508 growth (**Fig. 3**). Therefore, horizontal transmission to a few receivers followed by vertical
509 transmission by growth of infected receivers might be a more effective strategy to obtain more
510 infected receivers containing phage DNA.

511 Our results demonstrate that the rates of M13 phage-mediated intercellular gate activation
512 compare favourably against both small molecules and conjugation. Using isolated phages for
513 induction of our simplest circuit (NOT gate), we achieve 20% induction in 64 min (**Fig. 4c**),
514 compared to the 35–102 minutes using different concentrations of HSL molecules in previous
515 studies^{58,59}. Using phage-secreting sender cells to communicate with receivers in a co-culture,
516 we achieved 20% activation in 42 minutes (**Fig. S9.1**), which is faster than the 146 minutes
517 previously seen for AHL molecules⁶⁰. Due to the slow signal accumulation in sender-receiver
518 co-cultures, many small molecule communication experiments instead use conditioned media
519 for receiver activation⁶¹, or other specialised strategies to enrich signal accumulation⁹. Our
520 system demonstrated significant fold activation of circuits without such enrichment strategies:
521 21-fold (**Fig. 5d**), 17-fold (**Fig. 6d**), and 10-fold (**Fig. 6h**) for single-, dual-, and triple-input
522 circuits, respectively. However, these are lower than fold-changes of 15–200-fold seen with
523 2–4 input unicellular circuits using transcription factors or CRISPRi^{23,62}.

524 M13-mediated communication was faster than conjugation, with ~95% of receivers infected
525 within 5 hours (**Fig. 4d**), versus 50% in 6 hours using conjugation²⁷. This is reflected in the
526 transfer frequency obtained using M13 phages (**Fig. 4f**), which is about 5 orders of magnitude

527 higher than for conjugation²⁷. Furthermore, phage-mediated communication does not require
528 cell-to-cell contact, making it applicable even in sparse populations. Phage messages can
529 stay viable in harsh environments before they find a receiver cell for delivery⁶³. Unlike
530 conjugation that requires an active F-pilus as DNA conduit⁶⁴, M13 needs the F-pilus for the
531 initial surface attachment but not as a DNA conduit into the cell^{65,66}. As a result, M13 infection
532 can continue into the stationary phase of cell growth while conjugation cannot⁶⁷. In both cases,
533 cell surface receptors can be engineered to modify the transfer rates of both M13 transduction
534 and conjugation^{26,68}.

535 We combined phage-mediated communication with CRISPRi to develop the i-CRISPRi
536 system, implementing NOT and YES gates, as well as AND and AND-AND-NOT gates in co-
537 cultures with up to 4 cell types at a time. Our most complex circuit implemented, the AND-
538 AND-NOT gate, uses a dual-rail encoding with 3 sender strains (of 6 possible sender strains)
539 and 1 receiver strain in a co-culture. The ability of several -gp3 ϕ phages to simultaneously
540 infect the same receiver enables multiplex information processing, which is not possible using
541 many conjugation systems due to surface exclusion after the first transfer event⁶⁹. However,
542 conjugation can be used to re-transmit messages as receiver cells can assume the role of
543 senders after the initial message delivery²⁷. Due to gp3-mediated immunity⁴⁶, such re-
544 transmission is not normally possible for -gp3 ϕ phagemids but it is possible for +gp3 ϕ
545 phagemids, provided the receivers carry an appropriate helper. Alternatively, other solutions
546 that combine signal multiplexing with re-transmission could employ conditional expression of
547 *gp3* as done in stringency-modulated PACE⁷⁰.

548 Future enhancements to the M13 messaging system could include selective packaging of
549 orthogonal messages, targeting receivers with specific surface receptors⁶⁸, and combining the
550 system with re-addressable delivery of messages²⁷. Our data suggest that changing plasmid
551 replication origins can modulate secretion rates, thereby generating an array of messaging
552 variants with different communication properties. If only transient DNA delivery is required,
553 mini-phagemids with a split M13 packaging signal and no bacterial replication origin can be
554 employed⁷¹. For applications requiring both analogue and digital signals, small molecule
555 communication may be combined with conjugation- and phage-mediated DNA messaging.
556 The phage-mediated CRISPRi system developed in this work is amenable for interfacing with
557 other cellular communication systems, thereby expanding distributed computing circuits and
558 DNA delivery applications for microbiome engineering.

559

560

561 **Methods**

562 **Bacterial strains, growth conditions, and cloning**

563 All bacteria used in this study are *Escherichia coli* strains (**Table S1**). They were grown at
564 37 °C in LB media (liquid with shaking at 180 rpm, or solid LB plates with 1.5% w/v agar)
565 supplemented with the appropriate antibiotics at the following concentrations (unless
566 otherwise indicated): kanamycin (kan 30 µg mL⁻¹), ampicillin (amp 100 µg mL⁻¹), gentamycin
567 (gent 10 µg mL⁻¹), tetracycline (tet 10 µg mL⁻¹), and streptomycin (str 50 µg mL⁻¹);
568 concentrations were halved when using multiple antibiotics for selection. Strains and
569 antibiotics used are listed in **Table S1**.

570 To calculate the growth rates of strains, cells were diluted 100x from overnight cultures and
571 re-grown in a 96-well plate (200 µL per well) in a plate-reader (Biotek Synergy HTX) until they
572 reached an OD₆₀₀ of 0.2 to 0.3, following which they were diluted again by 40x into a new
573 plate. Cultures in the second plate were grown overnight, recording their OD₆₀₀ at 15 min
574 intervals. The data generated was used to calculate the Specific Growth Rates (µ).

575 Cloning was performed by Golden Gate Assembly of PCR-amplified DNA fragments using
576 NEB enzymes: Q5 DNA polymerase (#M0492), BsaI-HFv2 (#R3733), and T4 DNA ligase
577 (#M0202M). *E. coli* strains Dh5α and TOP10 were used for cloning. All plasmids constructed
578 were verified by Sanger sequencing. Plasmids used in this study are listed in **Table S2**, and
579 plasmid maps included with the Supplementary materials.

580 **Sender growth and phage preparation**

581 Sender strains (**Table S1**) were streaked on LBA plates (1.5% w/v agar) and grown
582 overnight at 37 °C. Single colonies were inoculated in 5 mL LB media with appropriate
583 antibiotics and incubated overnight at 37 °C, with 180 rpm shaking. Overnight cultures were
584 diluted 1000x in 100 mL fresh LB media with antibiotics and incubated for ~15 hours at 37 °C,
585 180 rpm. Periodically, optical density was recorded (OD₆₀₀; spectrophotometer UVisco V-
586 1100D) and 1 mL culture sample was spun down at 4500x g for 10 mins, supernatant was
587 filtered (0.22 µm filter, Millex SLGP033RS), and the resulting phage preps stored at 4 °C.
588 Phage titres at each time-point were estimated using CFU or PFU assays (see below).

589 **Phage counting**

590 *CFU assay*: Receiver cells (ER2738F) grown overnight were diluted 1000x and re-grown
591 at 37 °C in LB (with appropriate antibiotics) until they reached a spectrophotometer OD₆₀₀
592 between 1 and 1.5. Cells were chilled on ice for at least 30 min, and then 90 µL aliquoted into
593 eppendorf tubes. The tubes were moved to room temperature (RT) for 5 min before adding
594 phages to the cells. 10 µL of different phage dilutions (10⁻¹ to 10⁻¹⁴) were mixed with the
595 receiver cells and incubated at RT for 20 min. Thereafter, the mixtures were plated on LBA
596 plates with the appropriate antibiotic concentration. Colonies on the LBA plates were counted
597 the next day after incubation at 37 °C for ~16h. Colony counts from plates were used to
598 determine the mL⁻¹ titres of the phage preps according to the formula: CFU count / (phage
599 dilution * phage volume used in mL).

600 *PFU assay*: Receiver cells (ER2738F_HΔgIII) grown overnight were diluted 1000x and re-
601 grown at 37 °C in LB (tet+gent) until they reached a spectrophotometer OD₆₀₀ between 1 and
602 1.5. Cells were chilled on ice for at least 30 min, and then 90 µL aliquoted into eppendorf
603 tubes. The tubes were moved to RT shortly before mixing 10 µL of different phage dilutions
604 (10⁻¹ to 10⁻¹⁴) with the receiver cells, and then adding the mix to 10 mL of soft LBA (0.75% w/v
605 agar with 0.2 mM IPTG and 40 µg mL⁻¹ X-gal), previously aliquoted into a 15 mL tube and kept
606 molten at 50 °C. The phage+receiver mix in the soft agar was immediately poured onto a solid
607 plate with 20 mL hard LBA (1.5% w/v agar), and after the soft LBA had solidified the plate was
608 incubated at 37 °C for 16-24 h. Plaques of the non-lytic M13 phage are turbid/ diffused, usually
609 making them harder to see. IPTG and X-gal colours the plaques blue (LacZ ω in the F-plasmid
610 is complemented by the LacZ α in the phagemid), making them easier to visualise. Plaque
611 counts from plates were used to determine the mL⁻¹ titres of the phage preps according to the
612 formula: PFU count / (phage dilution * phage volume used in mL).

613 **Instantaneous Growth and Secretion Rate analysis**

614 Growth rates between two consecutive time-points were calculated according to the
615 following formula: Specific Growth Rate (μ) = $\ln(OD_2/OD_1) / (t_2-t_1)$, where OD₁ and OD₂ are
616 the OD₆₀₀ values at time-points t₁ and t₂.

617 Secretion rates between two consecutive time-points were calculated according to the
618 following formula: Secretion Rate = $\mu * (P_2-P_1) / (C_2-C_1)$, where P₁ and P₂ are the phage
619 concentrations and C₁ and C₂ are the cell concentrations at time-points t₁ and t₂. μ is the
620 specific growth rate calculated above. OD₆₀₀ of sender cells was converted to cell
621 concentration values using the fit in **Note S2 (Fig. S2.1)**.

622 **Receiver infection analysis**

623 To determine the effect of cell physiology on phage infection, receiver strain was streaked
624 on LBA plates(1.5% w/v agar) and grown overnight at 37 °C. Single colony was inoculated in
625 5 mL LB media with appropriate antibiotics and incubated overnight at 37 °C, with 180 rpm
626 shaking. Overnight cultures were diluted 1000x in 100 mL fresh LB media with antibiotics, and
627 incubated at 37 °C, 180 rpm. OD₆₀₀ of the culture was periodically monitored, and 10 mL
628 culture samples were stored at 4 °C when they reached ODs: 0.05, 0.1, 0.5, 1, 1.5, 2, 2.5.
629 Cultures were cooled on ice for at least 30 mins. Appropriate volumes of each culture sample
630 was spun down at 4500x g for 10 mins to wash pellets with LB media without antibiotics and
631 adjust (normalise) cell densities. These receiver culture samples were used for CFU and PFU
632 assays with the same phage concentrations.

633 To determine the effect of cell density on phage infection, receiver strain was streaked on
634 LBA plates (1.5% w/v agar) and grown overnight at 37 °C. Single colony was inoculated in 5
635 mL LB media with appropriate antibiotics and incubated overnight at 37 °C, 180 rpm. Overnight
636 cultures were diluted 1000x in 25 mL fresh LB media with antibiotics and incubated at 37 °C,
637 180 rpm, till the OD₆₀₀ reached ~1.5. Culture was cooled on ice for at least 30 mins and then
638 spun down at 4500 RCF for 10 mins to wash pellets with LB media without antibiotics. Culture
639 was adjusted to different densities 0.05, 0.1, 0.5, 1, 2, 3, 4 and 5. These receiver cultures were
640 used for CFU and PFU assays with the same phage concentrations.

641 **Receiver infection in growing conditions and quantifying unadsorbed phages**

642 For the infection plate-reader experiments, overnight cultures of receiver cells (ER2738F)
643 were diluted 1000x and re-grown to a spectrophotometer OD₆₀₀ of 0.6-0.7, following which
644 they were cooled on ice for ~30 min and their OD₆₀₀ re-adjusted to different densities (0.25,
645 0.125, 0.0625, 0.03125) while still on ice. Several serial dilutions (3^N-fold, N = 0 to 10) of the
646 phage prep (pSB1K3_LacZα_gIII_M13ps, undiluted concentration of 36.2x10⁵ PFU mL⁻¹), and
647 a no-phage control, were prepared and 45 μL aliquoted into a 96-well plate at RT. 150 μL of
648 the different receiver dilutions were added to the plate and incubated at RT for 20 min. Next,
649 5 μL of LB was added to each well, without or with kanamycin (end concentration 30 μg mL⁻¹
650 ¹), and the plate incubated overnight in a plate-reader (Biotek Synergy HTX) at 37 °C, 205
651 cpm, while recording OD₆₀₀ at 15 min intervals. The above experiments were repeated four
652 times, each with a different set of phage dilutions added to the plate: (a) 3x technical replicates
653 of dilutions 3⁸-3¹⁰ and the no-phage control (continuous), (b) 3x technical replicates of dilutions
654 3¹-3³ and the no-phage control (continuous), (c) 3x technical replicates of dilutions 3¹-3³ and
655 the no-phage control (discontinuous), and (d) single replicate of dilutions 3⁰-3¹⁰ and the no-
656 phage control (continuous).

657 In the discontinuous run above, the plate was paused at several time-points (2, 6, and 10
658 h) to draw a 3 μL sample from each well of the third column (phage dilution 3²), which was
659 added to 200 μL of LB (+gent) to kill all cells and later used to quantify by PFU assay the
660 unadsorbed phages in the well. The pauses for phage sampling resulted in an average gap of
661 ~45 min between plate reader measurements before and after the pause, which was taken
662 into account for plotting OD vs time curves.

663 **Phage mediated sender-to-receiver communication in co-cultures**

664 For the communication plate-reader experiments, an overnight culture of receiver cells
665 (ER2738F) was diluted 1000x and re-grown to a spectrophotometer OD₆₀₀ of 0.4, following
666 which it was cooled on ice for ~30 min and several OD₆₀₀ dilutions made (0.136, 0.068, 0.034,
667 and 0.0) while still on ice. Overnight culture of senders (TOP10_H_gIII-KanΦ and TOP10_H_
668 KanΦ) was diluted 500x and re-grown to a spectrophotometer OD₆₀₀ of 0.2, following which it
669 was cooled on ice for ~30 min and several OD₆₀₀ dilutions made (0.125, 0.062, 0.031, 0.015,
670 0.007, and 0.0) while still on ice. 90 μL of receiver cell dilutions were added per well to a 96-
671 well plate in quadruplet (for the four different growth conditions), followed by 90 μL of the
672 sender cell dilutions also in quadruplet. The plate was run at 37 °C for 1 h, following which 20
673 μL of LB with the appropriate antibiotics (10x concentrated, to achieve the 1x end-
674 concentration) was added to each well, and the plate was grown overnight at 37 °C, 205 cpm,
675 while recording OD₆₀₀ at 15 min intervals.

676 **Receiver infection CRISPRi time lapse in growing conditions**

677 Receiver strain (carrying F⁺-plasmid + dCas9-GFP plasmid) and sender strains (carrying
678 helper plasmid + sgRNA phagemid) were streaked on LBA plates (1.5% w/v agar), with
679 appropriate antibiotics, and grown overnight at 37 °C. Single colonies were inoculated in 5 mL
680 LB media with appropriate antibiotics and incubated overnight at 37 °C, with 180 rpm shaking.
681 Overnight cultures were diluted 1000x in 100 mL fresh LB media with antibiotics and incubated
682 at 37 °C, 180 rpm, until they reached OD₆₀₀ ~0.3. Cultures were cooled on ice for at least 30

683 mins, pellets were washed and several dilutions made with different ODs (0.12, 0.06, 0.03,
684 and 0.0), while still on ice. The supernatant was filtered through 0.22 μm filters to collect
685 phages and several serial dilutions were made (10x, 20x, 40x, 0). 100 μL of receiver cultures
686 were mixed with 100 μL of sender cultures in a 96-well plate and grown in plate reader for 5
687 hours with no antibiotic, while recording OD_{600} and GFP fluorescence at 15 min intervals. At
688 0, 1, 2, 3, 4 and 5 hours, 10 μL co-culture was added to 1x PBS containing 2 mg mL^{-1}
689 kanamycin to stop protein expression and kill the cells. Following this, the cells in 1x PBS +
690 kan (2 mg mL^{-1}) were stored at 4 $^{\circ}\text{C}$ for later flow cytometry analysis.

691 **Phage transfer frequency calculations**

692 Transfer frequencies were calculated from the co-culturing flow cytometry data in **Fig. 4d-**
693 **e** and **S6.2**. The events recorded at each time-point were gated by fluorescence to obtain the
694 number of cells of each type: senders (S, no GFP), uninfected receivers (Ru, GFP ON) and
695 infected receivers (Ri, GFP OFF). The transfer frequency was calculated as $R_i/S*(R_i+R_u)$,
696 according to the formula used to obtain transconjugant frequency in conjugation
697 experiments²⁷.

698 **Single input CRISPRi biological circuits**

699 Receiver strain (carrying F'-plasmid + dCas9-GFP plasmid) and sender strains (carrying
700 helper plasmid + sgRNA phagemid) were streaked on LBA plates (1.5% w/v agar), with
701 appropriate antibiotics, and grown overnight at 37 $^{\circ}\text{C}$. Single colonies were inoculated in 5 mL
702 LB media with appropriate antibiotics and incubated overnight at 37 $^{\circ}\text{C}$, with 180 rpm shaking.
703 Overnight cultures were diluted 1000x in 100 mL fresh LB media with antibiotics and incubated
704 at 37 $^{\circ}\text{C}$, 180 rpm, until they reached $\text{OD}_{600} \sim 0.3$. Cultures were cooled on ice for at least 30
705 mins, spun down and washed. Several dilutions made to different ODs (0.12, 0.06, 0.03, 0.01,
706 0.007 and 0.0), while still on ice. 90 μL of receiver cell dilutions were added per well to a 96-
707 well plate in quadruplet (for the four different growth conditions), followed by 90 μL of the
708 sender cell dilutions also in quadruplet. The plate was run at 37 $^{\circ}\text{C}$ for 4 h, while recording
709 OD_{600} and GFP fluorescence at 15 min intervals, following which 20 μL of LB with the
710 appropriate antibiotics (10x concentrated, to achieve the 1x end-concentration) was added to
711 each well, and the plate was grown overnight at 37 $^{\circ}\text{C}$, 205 rpm, while recording OD_{600} and
712 GFP fluorescence at 15 min intervals. After 16 hours of growth in selection media, 10 μL of
713 cultures were transferred to PBS for flow cytometry analysis performed immediately
714 afterwards.

715 **Multi-input CRISPRi biological circuits**

716 Receiver strain (carrying F-plasmid + dCas9-GFP plasmid) and sender strains (carrying
717 helper plasmid + sgRNA phagemid) were streaked on LBA plates (1.5% w/v agar), with
718 appropriate antibiotics, and grown overnight at 37 $^{\circ}\text{C}$. Single colonies were inoculated in 5 mL
719 LB media with appropriate antibiotics and incubated overnight at 37 $^{\circ}\text{C}$, with 180 rpm shaking.
720 Overnight cultures were diluted 1000x in 100 mL fresh LB media with antibiotics and incubated
721 at 37 $^{\circ}\text{C}$, 180 rpm, until they reached $\text{OD}_{600} \sim 0.3$. Cultures were cooled on ice for at least 30
722 mins, spun down and washed. Several dilutions made to different ODs (0.12, 0.06, 0.03, and
723 0.0), while still on ice. 100 μL of receiver cell dilutions were added per well to a 96-well plate,
724 followed by 100 μL (total) of the sender cell dilutions. For the 2-input gate, 50 μL each of the

725 2 sender dilutions was mixed together before adding to the receivers. For the 3-input gate,
726 33.3 μL each of the 3 sender dilutions was mixed together before adding to the receivers. The
727 plate was run at 37 °C for 4 h, while recording OD_{600} and GFP fluorescence at 15 min intervals,
728 following which the co-culture was diluted 20x in 200 μL fresh LB media with antibiotics,
729 selecting only infected receivers. The plate was grown overnight while recording OD_{600} and
730 GFP fluorescence at 15 min intervals. After 16 hours of growth in selection media, cultures
731 were used to prepare PBS+kan plates for flow cytometer analysis performed immediately
732 afterwards.

733 **Flow cytometry analysis**

734 Flow cytometry samples containing cells in 1x PBS (with 2 mg mL^{-1} of kanamycin) were
735 analysed using the Attune NxT flow cytometer (Thermofisher) equipped with a Cytkick
736 autosampler. Samples were fed into the flow cytometer using 96-well plates. ~20,000 bacterial
737 events were recorded per sample, excluding dead cells and debris from the analysis using
738 FSC and SSC thresholds of 100. GFP fluorescence was measured using excitation by a 488
739 nm laser and a 530/30 nm filter (BL1 channel). Voltages used were FSC: 265, SSC: 273, BL1:
740 278, for all experiments. Data collected were analysed using Attune Cytometric v5.3, and
741 plotted using python scripts. Flow cytometry overlays were plotted using the online tool:
742 floreada.io

743 **Acknowledgements**

744 We thank Jean-Loup Faulon for generous access to laboratory equipment. We thank
745 Alfonso Jaramillo for the kind gift of bacterial strains and plasmids. We thank Vijai Singh and
746 Sai Akhil Golla for their help in cloning some plasmids used in this study. We thank Hadi Jbara,
747 Roman Luchko, Tom Zaplana, and Anchita Sharma for technical assistance with M13 phage
748 protocols. We acknowledge the use of GPT-4o (Open AI, <https://chatgpt.com/>) for text editing
749 / rephrasing. We acknowledge support from the Digicosme working group HicDiesMeus, Ile-
750 de-France (IdF) region's DIM-RFSI (project COMBACT), INS2I CNRS (project BACON),
751 Université Paris-Saclay's STIC department (project DEPEC MODE), and INRAE's MICA
752 department (starting grant and project PHEMO). This research was funded in part by the
753 French National Research Agency (ANR) under the projects DREAMY (ANR-21-CE48-0003),
754 and PEPR Tbox4BioProd (ANR-22-PEBB-0012).

755 **Author contributions**

756 M.F., T.N., and M.K. conceived the study.
757 A.Pu., A.Pat., and M.K. designed the wet-lab experiments.
758 A.Pu., A.Pat., C.H., A.Pan., and M.K. performed the wet-lab experiments.
759 A.Pu., A.Pat., M.F., T.N., and M.K. analysed the data.
760 M.F., T.N., and M.K. acquired the funding.
761 A.Pu. and M.K. wrote the manuscript with contributions from all authors.
762 All authors read and approved the final manuscript.

763

764

765 **References**

766

- 767 1. Wan, X. *et al.* Cascaded amplifying circuits enable ultrasensitive cellular sensors for
768 toxic metals. *Nat. Chem. Biol.* **15**, 540–548 (2019).
- 769 2. Courbet, A., Endy, D., Renard, E., Molina, F. & Bonnet, J. Detection of pathological
770 biomarkers in human clinical samples via amplifying genetic switches and logic gates.
771 *Sci. Transl. Med.* **7**, 289ra83 (2015).
- 772 3. Kemmer, C. *et al.* Self-sufficient control of urate homeostasis in mice by a synthetic
773 circuit. *Nat. Biotechnol.* **28**, 355–360 (2010).
- 774 4. Bonnet, J., Yin, P., Ortiz, M. E., Subsoontorn, P. & Endy, D. Amplifying genetic logic
775 gates. *Science* **340**, 599–603 (2013).
- 776 5. Wang, B., Kitney, R. I., Joly, N. & Buck, M. Engineering modular and orthogonal genetic
777 logic gates for robust digital-like synthetic biology. *Nat. Commun.* **2**, 508 (2011).
- 778 6. Moon, T. S., Lou, C., Tamsir, A., Stanton, B. C. & Voigt, C. A. Genetic programs
779 constructed from layered logic gates in single cells. *Nature* **491**, 249–253 (2012).
- 780 7. Wang, B. & Buck, M. Customizing cell signaling using engineered genetic logic circuits.
781 *Trends Microbiol.* **20**, 376–384 (2012).
- 782 8. Santos-Moreno, J. & Schaerli, Y. CRISPR-based gene expression control for synthetic
783 gene circuits. *Biochem. Soc. Trans.* **48**, 1979–1993 (2020).
- 784 9. Tamsir, A., Tabor, J. J. & Voigt, C. A. Robust multicellular computing using genetically
785 encoded NOR gates and chemical ‘wires’. *Nature* **469**, 212–215 (2011).
- 786 10. Regot, S. *et al.* Distributed biological computation with multicellular engineered
787 networks. *Nature* **469**, 207–211 (2011).
- 788 11. Toda, S., Blauch, L. R., Tang, S. K. Y., Morsut, L. & Lim, W. A. Programming self-
789 organizing multicellular structures with synthetic cell-cell signaling. *Science* **361**, 156–
790 162 (2018).
- 791 12. Chuang, J. S. Engineering multicellular traits in synthetic microbial populations. *Curr.*
792 *Opin. Chem. Biol.* **16**, 370–378 (2012).

- 793 13. Grozinger, L. *et al.* Pathways to cellular supremacy in biocomputing. *Nat. Commun.* **10**,
794 5250 (2019).
- 795 14. Chen, Y. C., Destouches, L., Cook, A. & Fedorec, A. J. H. Synthetic microbial ecology:
796 engineering habitats for modular consortia. *J. Appl. Microbiol.* **135**, (2024).
- 797 15. Kylilis, N., Tuza, Z. A., Stan, G.-B. & Polizzi, K. M. Tools for engineering coordinated
798 system behaviour in synthetic microbial consortia. *Nat. Commun.* **9**, 2677 (2018).
- 799 16. Du, P. *et al.* De novo design of an intercellular signaling toolbox for multi-channel cell-
800 cell communication and biological computation. *Nat. Commun.* **11**, 4226 (2020).
- 801 17. Makri Pistikou, A.-M. *et al.* Engineering a scalable and orthogonal platform for synthetic
802 communication in mammalian cells. *Nat. Commun.* **14**, 7001 (2023).
- 803 18. Canadell, D. *et al.* Implementing re-configurable biological computation with distributed
804 multicellular consortia. *Nucleic Acids Res.* **50**, 12578–12595 (2022).
- 805 19. Mittelbrunn, M. & Sánchez-Madrid, F. Intercellular communication: diverse structures for
806 exchange of genetic information. *Nat. Rev. Mol. Cell Biol.* **13**, 328–335 (2012).
- 807 20. Soucy, S. M., Huang, J. & Gogarten, J. P. Horizontal gene transfer: building the web of
808 life. *Nat. Rev. Genet.* **16**, 472–482 (2015).
- 809 21. Hassan, F., Kamruzzaman, M., Mekalanos, J. J. & Faruque, S. M. Satellite phage TLC ϕ
810 enables toxigenic conversion by CTX phage through dif site alteration. *Nature* **467**, 982–
811 985 (2010).
- 812 22. López-Igual, R., Bernal-Bayard, J., Rodríguez-Patón, A., Ghigo, J.-M. & Mazel, D.
813 Engineered toxin-intein antimicrobials can selectively target and kill antibiotic-resistant
814 bacteria in mixed populations. *Nat. Biotechnol.* **37**, 755–760 (2019).
- 815 23. Nielsen, A. A. K. & Voigt, C. A. Multi-input CRISPR/Cas genetic circuits that interface
816 host regulatory networks. *Mol. Syst. Biol.* **10**, 763 (2014).
- 817 24. Takahashi, M. K. & Lucks, J. B. A modular strategy for engineering orthogonal chimeric
818 RNA transcription regulators. *Nucleic Acids Res.* **41**, 7577–7588 (2013).
- 819 25. Brophy, J. A. N. *et al.* Engineered integrative and conjugative elements for efficient and

- 820 inducible DNA transfer to undomesticated bacteria. *Nat Microbiol* **3**, 1043–1053 (2018).
- 821 26. Robledo, M. *et al.* Targeted bacterial conjugation mediated by synthetic cell-to-cell
822 adhesions. *Nucleic Acids Res.* **50**, 12938–12950 (2022).
- 823 27. Marken, J. P. & Murray, R. M. Addressable and adaptable intercellular communication
824 via DNA messaging. *Nat. Commun.* **14**, 2358 (2023).
- 825 28. Krom, R. J., Bhargava, P., Lobritz, M. A. & Collins, J. J. Engineered Phagemids for
826 Nonlytic, Targeted Antibacterial Therapies. *Nano Lett.* **15**, 4808–4813 (2015).
- 827 29. Libis, V. K. *et al.* Silencing of antibiotic resistance in *E. coli* with engineered phage
828 bearing small regulatory RNAs. *ACS Synth. Biol.* **3**, 1003–1006 (2014).
- 829 30. Hsu, B. B. *et al.* In situ reprogramming of gut bacteria by oral delivery. *Nat. Commun.*
830 **11**, 5030 (2020).
- 831 31. Brödel, A. K. *et al.* In situ targeted base editing of bacteria in the mouse gut. *Nature* **632**,
832 877–884 (2024).
- 833 32. Tao, W. *et al.* In Vitro Packaging Mediated One-Step Targeted Cloning of Natural
834 Product Pathway. *ACS Synth. Biol.* **8**, 1991–1997 (2019).
- 835 33. Correa, A. M. S. *et al.* Revisiting the rules of life for viruses of microorganisms. *Nat.*
836 *Rev. Microbiol.* **19**, 501–513 (2021).
- 837 34. Hay, I. D. & Lithgow, T. Filamentous phages: masters of a microbial sharing economy.
838 *EMBO Rep.* **20**, (2019).
- 839 35. Smeal, S. W., Schmitt, M. A., Pereira, R. R., Prasad, A. & Fisk, J. D. Simulation of the
840 M13 life cycle I: Assembly of a genetically-structured deterministic chemical kinetic
841 simulation. *Virology* **500**, 259–274 (2017).
- 842 36. Kim, I., Moon, J.-S. & Oh, J.-W. Recent advances in M13 bacteriophage-based optical
843 sensing applications. *Nano Converg* **3**, 27 (2016).
- 844 37. Smith, G. P. & Scott, J. K. Libraries of peptides and proteins displayed on filamentous
845 phage. *Methods Enzymol.* **217**, 228–257 (1993).
- 846 38. Davenport, B. J. *et al.* Phage-like particle vaccines are highly immunogenic and protect

- 847 against pathogenic coronavirus infection and disease. *NPJ Vaccines* **7**, 57 (2022).
- 848 39. Sedki, M., Chen, X., Chen, C., Ge, X. & Mulchandani, A. Non-lytic M13 phage-based
849 highly sensitive impedimetric cytosensor for detection of coliforms. *Biosens. Bioelectron.*
850 **148**, 111794 (2020).
- 851 40. Esvelt, K. M., Carlson, J. C. & Liu, D. R. A system for the continuous directed evolution
852 of biomolecules. *Nature* **472**, 499–503 (2011).
- 853 41. Brödel, A. K., Jaramillo, A. & Isalan, M. Engineering orthogonal dual transcription factors
854 for multi-input synthetic promoters. *Nat. Commun.* **7**, 13858 (2016).
- 855 42. Ortiz, M. E. & Endy, D. Engineered cell-cell communication via DNA messaging. *J. Biol.*
856 *Eng.* **6**, 16 (2012).
- 857 43. Tzagoloff, H. & Pratt, D. THE INITIAL STEPS IN INFECTION WITH COLIPHAGE M13.
858 *Virology* **24**, 372–380 (1964).
- 859 44. De Paepe, M., De Monte, S., Robert, L., Lindner, A. B. & Taddei, F. Emergence of
860 variability in isogenic *Escherichia coli* populations infected by a filamentous virus. *PLoS*
861 *One* **5**, e11823 (2010).
- 862 45. Mai-Prochnow, A. *et al.* Big things in small packages: the genetics of filamentous phage
863 and effects on fitness of their host. *FEMS Microbiol. Rev.* **39**, 465–487 (2015).
- 864 46. Boeke, J. D., Model, P. & Zinder, N. D. Effects of bacteriophage f1 gene III protein on
865 the host cell membrane. *Mol. Gen. Genet.* **186**, 185–192 (1982).
- 866 47. Ploss, M. & Kuhn, A. Kinetics of filamentous phage assembly. *Phys. Biol.* **7**, 045002
867 (2010).
- 868 48. Jahn, M., Vorpahl, C., Hübschmann, T., Harms, H. & Müller, S. Copy number variability
869 of expression plasmids determined by cell sorting and Droplet Digital PCR. *Microb. Cell*
870 *Fact.* **15**, 211 (2016).
- 871 49. Kick, B., Hensler, S., Praetorius, F., Dietz, H. & Weuster-Botz, D. Specific growth rate
872 and multiplicity of infection affect high-cell-density fermentation with bacteriophage M13
873 for ssDNA production. *Biotechnol. Bioeng.* **114**, 777–784 (2017).

- 874 50. Tomoeda, M., Inuzuka, M. & Date, T. Bacterial sex pili. *Prog. Biophys. Mol. Biol.* **30**, 23–
875 56 (1975).
- 876 51. Billiard, S., Collet, P., Ferrière, R., Méléard, S. & Tran, V. C. The effect of competition
877 and horizontal trait inheritance on invasion, fixation, and polymorphism. *J. Theor. Biol.*
878 **411**, 48–58 (2016).
- 879 52. Bloxham, B., Lee, H. & Gore, J. Diauxic lags explain unexpected coexistence in multi-
880 resource environments. *Mol. Syst. Biol.* **18**, e10630 (2022).
- 881 53. Wang, H., La Russa, M. & Qi, L. S. CRISPR/Cas9 in Genome Editing and Beyond.
882 *Annu. Rev. Biochem.* **85**, 227–264 (2016).
- 883 54. Nordholt, N., van Heerden, J., Kort, R. & Bruggeman, F. J. Effects of growth rate and
884 promoter activity on single-cell protein expression. *Sci. Rep.* **7**, 6299 (2017).
- 885 55. Lim, J. J. *et al.* Growth phase estimation for abundant bacterial populations sampled
886 longitudinally from human stool metagenomes. *Nat. Commun.* **14**, 5682 (2023).
- 887 56. Porter, N. T. *et al.* Phase-variable capsular polysaccharides and lipoproteins modify
888 bacteriophage susceptibility in *Bacteroides thetaiotaomicron*. *Nat Microbiol* **5**, 1170–
889 1181 (2020).
- 890 57. Lourenço, M. *et al.* The Spatial Heterogeneity of the Gut Limits Predation and Fosters
891 Coexistence of Bacteria and Bacteriophages. *Cell Host Microbe* **28**, 390–401.e5 (2020).
- 892 58. Daer, R. *et al.* Characterization of diverse homoserine lactone synthases in *Escherichia*
893 *coli*. *PLoS One* **13**, e0202294 (2018).
- 894 59. Ábrahám, Á. *et al.* Single-cell level LasR-mediated quorum sensing response of
895 *Pseudomonas aeruginosa* to pulses of signal molecules. *Sci. Rep.* **14**, 16181 (2024).
- 896 60. Silva, K. P., Chellamuthu, P. & Boedicker, J. Q. Signal Destruction Tunes the Zone of
897 Activation in Spatially Distributed Signaling Networks. *Biophys. J.* **112**, 1037–1044
898 (2017).
- 899 61. Tekel, S. J. *et al.* Engineered Orthogonal Quorum Sensing Systems for Synthetic Gene
900 Regulation in *Escherichia coli*. *Front Bioeng Biotechnol* **7**, 80 (2019).

- 901 62. Moon, T. S., Lou, C., Tamsir, A., Stanton, B. C. & Voigt, C. A. Genetic programs
902 constructed from layered logic gates in single cells. *Nature* **491**, 249–253 (2012).
- 903 63. Branston, S. D., Stanley, E. C., Ward, J. M. & Keshavarz-Moore, E. Determination of the
904 survival of bacteriophage M13 from chemical and physical challenges to assist in its
905 sustainable bioprocessing. *Biotechnol. Bioprocess Eng.* **18**, 560–566 (2013).
- 906 64. Goldlust, K. *et al.* The F pilus serves as a conduit for the DNA during conjugation
907 between physically distant bacteria. *Proc. Natl. Acad. Sci. U. S. A.* **120**, e2310842120
908 (2023).
- 909 65. Lubkowski, J., Hennecke, F., Plückthun, A. & Wlodawer, A. Filamentous phage
910 infection: crystal structure of g3p in complex with its coreceptor, the C-terminal domain
911 of TolA. *Structure* **7**, 711–722 (1999).
- 912 66. Russel, M., Whirlow, H., Sun, T. P. & Webster, R. E. Low-frequency infection of F-
913 bacteria by transducing particles of filamentous bacteriophages. *J. Bacteriol.* **170**, 5312–
914 5316 (1988).
- 915 67. Frost, L. S. & Manchak, J. F- phenocopies: characterization of expression of the F
916 transfer region in stationary phase. *Microbiology* **144 (Pt 9)**, 2579–2587 (1998).
- 917 68. Lorenz, S. H. & Schmid, F. X. Reprogramming the infection mechanism of a filamentous
918 phage. *Mol. Microbiol.* **80**, 827–834 (2011).
- 919 69. Achtman, M., Kennedy, N. & Skurray, R. Cell–cell interactions in conjugating
920 *Escherichia coli*: role of traT protein in surface exclusion. *Proc. Natl. Acad. Sci. U. S. A.*
921 **74**, 5104–5108 (1977).
- 922 70. Carlson, J. C., Badran, A. H., Guggiana-Nilo, D. A. & Liu, D. R. Negative selection and
923 stringency modulation in phage-assisted continuous evolution. *Nat. Chem. Biol.* **10**,
924 216–222 (2014).
- 925 71. Wong, S., Jimenez, S. & Slavcev, R. A. Construction and characterization of a novel
926 miniaturized filamentous phagemid for targeted mammalian gene transfer. *Microb. Cell*
927 *Fact.* **22**, 124 (2023).